PRAMANA — journal of physics

Vol. 79, No. 6
December 2012
pp. 1425–1441

Generation of tunable 16 μm radiation from CO_2 by cascade lasing

UTPAL NUNDY[1,*] and MANOJ KUMAR[2]

[1]BH-2–76, Kendriya Vihar, Kharghar, Sector-11, Navi Mumbai 410 210, India
[2]Laser Material Processing Division, Raja Ramanna Centre for Advanced Technology, Indore 452 013, India
*Corresponding author. E-mail: unundy@yahoo.co.in

MS received 10 December 2011; revised 18 May 2012; accepted 29 May 2012

Abstract. In this paper we propose a scheme to generate tunable 16 μm radiation from CO_2 molecules by cascade lasing. The stimulating 9.5 μm radiation is generated internally by the fast rotating mirror Q-switching technique. The optical scheme proposed by us uses an intracavity prism to separate the 9.5 μm and the 16 μm beams. This facilitates independent tuning of the two beams if required. In the present configuration, only the 16 μm cavity is dispersive. The 9.5 μm beam grows spontaneously in a stable semiconfocal resonator. We have developed a theoretical model to simulate the proposed scheme. The model predicts the energy and power of 16 μm radiation. The calculated values are much higher than the previously obtained experimental values. The results point out the feasibility of developing a laser system based on the theoretical design parameters presented in this paper. Such laser systems can find application in uranium isotope separation studies.

Keywords. Generation of 16 μm radiation from CO_2 molecules; E-beam controlled discharge; uranium laser isotope separation.

PACS Nos 42.55.Lt; 42.60.Gd; 52.80.−s

1. Introduction

A tunable 16 μm laser [1] has potential application in the field of laser isotope separation [2–4]. The tunable 16 μm laser can be operated on the $(02^00–01^10)$ transition in CO_2 which is centred at 16.2 μm. The first step is to produce a population inversion between the (00^01) and the (02^00) levels of CO_2. Wexler *et al* [5] and Krupke [6] achieved this by creating vibration excitation in a N_2 and He gas mixture using a glow discharge, expanding this gas mixture in a supersonic nozzle and mixing cool CO_2 in the supersonic region thereby transferring the vibration energy of N_2 to the CO_2 (00^01) level. Kasner *et al* [7,8] used a pulsed electrical discharge to excite a cryogenically-cooled CO_2 laser–gas mixture,

DOI: 10.1007/s12043-012-0346-x; ***e*Publication: 31 August 2012**

and achieved maximum inversion between the (00^01) and the (02^00) levels of CO_2 in the afterglow period. Osgood [1] used optical pumping of CO_2 by a HBr laser to achieve this inversion. The second step is to saturate the (00^01–02^00) transition so that half of the inversion density will be added to the (02^00) level, thereby creating a population inversion between (02^00) and (01^10) levels. It is possible to achieve this saturation by (1) injecting a stimulating laser pulse operating on 9.6 μm from an external CO_2 laser [7,8] or by (2) generating the 9.6 μm pulse internally by the rotating mirror Q-switch [5,6]. In the latter scheme, the laser first emits a 9.6 μm pulse, followed by the 16 μm pulse. This mode of operation is called cascade lasing. Among the two schemes, the one using cascade lasing avoids the use of an external laser and hence improves the overall efficiency of the laser system. Cooling of the gas mixture helps in lowering the thermal population of the (01^10) level.

The 16 μm CO_2 laser operates optimally with a He-rich gas mixture with low CO_2 content and low gas pressure. Because of Fermi resonance there is a rapid deactivation of the population of the (02^00) level. This restricts the maximum CO_2 partial pressure in the laser–gas mixture. This severely limits the output energy and power of this laser. Large lasing volume is therefore required to generate energy and power at useful levels. Electron beam controlled transverse discharges are scalable and are appropriate for the excitation of cryogenically-cooled 16 μm laser–gas mixtures [9].

In this paper, we propose a scheme for generating tunable 16 μm laser radiation from CO_2 molecules by cascade lasing. The laser uses a large-aperture electron beam-controlled transverse discharge. The 9.6 μm beam is generated internally by the rotating mirror Q-switch. Radiation of 16 μm wavelength is generated collinearly with the 9.6 μm wavelength. The dual wavelength cavity utilizes an intracavity prism to split the 9.6 μm and 16 μm beams [6]. The 16 μm laser is tuned by utilizing a grating. The 9.6 μm cavity is a stable resonator semiconfocal cavity comprising of a curved mirror and a plane mirror. The proposed laser is similar to that of Kasner [7,8] who have used high voltage pulse in longitudinally pumped laser. However, in our case transverse discharge configuration is used. Due to the longitudinal configuration used by Kasner, operating pressure of the gas mixture was restricted to $\sim$10 Torr. The operating pressure in our case is 100 Torr due to the transverse excitation of discharge medium. The higher pressure improves significantly the peak power of the 9.6 μm stimulating laser pulse, and helps in improving the energy and power of the 16 μm pulse. Chatterjee and Nath [10] developed a theoretical model to simulate the experimental conditions of Kasner *et al* [7]. Good agreement was obtained with experimental results. They had predicted that use of transverse discharge and operation at higher pressure should improve the peak power of the 16 μm laser considerably. When the 9.6 μm beam is more powerful, it can compensate for the larger collisional relaxation of the (02^00) level at higher pressure, and thus allow operation at higher gas pressures. We have extended the earlier theoretical model of Chatterjee and Nath [10] and have also included simulation of the discharge and Q-switching of the laser in our model.

We present the results of the theoretical model to generate 16 μm laser with high energy from a transversely excited electron beam-controlled electrical discharge in He-rich gas mixture. The basic intention is to indicate theoretically the capability of the proposed scheme. No experimental work has been carried out yet on the proposed scheme, but we have compared the result of our prediction regarding the 9.5 μm Q-switched pulse with

actual experimental results of Sakai and Hamada [11], who have developed a high-power Q-switched CO_2 laser. A close match between theoretically predicted values and their experimental results conveys the accuracy of the model and hence realistic theoretical predictions of 16 μm radiation from a similar system if designed on these lines.

2. Our scheme

Figure 1 is the schematic diagram of the proposed set-up for the tunable 16 μm laser. The gas mixture used is a He-rich mixture containing CO_2, N_2 and He in the ratio 1 : 1 : 40 at a pressure of 100 Torr. The mixture is assumed to be at a temperature of -150°C. Three e-beam controlled discharges (shown in figure 1 as discharge modules D1, D2 and D3) provide optimum excitation to the gas mixture [9]. The 9.5 μm cavity is formed by the fully reflecting curved mirror M1 of 10 m radius of curvature and the plane output coupler OC. Reflectivity of the output coupler is 98% at 9.5 μm. The Q-switching is obtained by rotating an intracavity fully reflecting plane mirror M2 at 400 Hz. The 9.5 μm cavity contains a 10.6 μm absorber cell C, containing SF_6 or BCl_3 to prevent lasing at 10.6 μm. The estimated temperature of the discharge-heated gas mixture is 200 K. At this temperature the rotational level $J = 13$ corresponding to 00^01 upper laser level of CO_2 will have the maximum population. This makes the 9.6 $P(14)$ line as the strongest line, which will lase in preference to other lines and grow spontaneously. This line operates at 9.5 μm wavelength. The 9.5 μm radiation will stimulate lasing at 16 μm. The intracavity KBr prism separates the paths of the 9.5 and 16 μm beams. This allows use of a grating for tuning the 16 μm laser. The 16 μm cavity is formed by the mirrors M1, M2 and grating G. It is assumed that the grating has 85% efficiency. The 16 μm laser output is taken from one of the gratings orders. It is assumed that 10% of the internal 16 μm energy can be coupled out in this order.

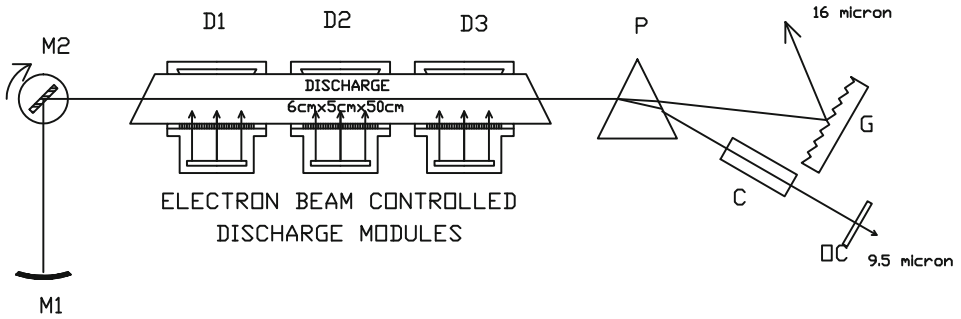

Figure 1. Schematic of the set-up for the 16 μm laser. M1 – fully reflecting curved mirror of 10 m radius of curvature, M2 – fully reflecting rotating plane mirror, D1, D2, D3 – electron beam-controlled discharge modules, with discharge dimension 6 cm × 5 cm × 50 cm, P – KBr prism, G – 60 lines/mm grating with 85% efficiency, C – SF_6 cell, OC – output coupler with 98% reflectivity.

3. Mode of operation

3.1 *Electron beam-controlled discharge modules*

The electron beam is generated by a cold cathode gun energized by a pulse forming network (PFN) based power supply. The power supply provides a -300 kV, 250 A pulse with 1.5 μs duration. The area of the electron beam is of 5×50 cm^2. The electron beam passes through a 25 μm Al foil and its support structure to sustain the main discharge. The main discharge is driven by a capacitor of 0.7 μF charged to 6 kV. The main discharge electrodes are separated by 6 cm. The discharge has a dimension of $6 \times 5 \times 50$ cm^3. The electron beam provides a current density of 330 mA cm^{-2} in the discharge region. The main discharge is initiated 500 ns after the application of electron beam voltage. The main discharge persists till 12 μs and deposits $\sim$12.5 J energy in the discharge. The discharge energy density is $\sim$65 J l^{-1}atm^{-1}. After the application of the discharge one allows a relaxation of excited active medium for a duration of 30 μs. During this afterglow period, the (00^01) level attains maximum population due to resonant transfer from N_2 ($v = 1$) level. All other low-lying levels which were populated during the discharge relax back almost to their thermal levels. The Q-switching is arranged to occur just at this time.

3.2 *Rotating mirror Q-switching*

The 9.5 μm cavity consisting of mirrors M1 (10 m radius of curvature) and OC (plane) is a semiconfocal cavity. The distance between the two mirrors is 5 m. The diameter of each mirror is 5 cm. Let us first consider a semiconfocal cavity consisting of a curved mirror and a plane mirror and let the curved mirror rotate. The optic axis of this resonator is defined as the line which is perpendicular to the plane mirror and which intersects the pole of the curved mirror. If the curved mirror is rotated, this optic axis will move within the optical cavity parallel to itself [12]. In the configuration adopted by us, we keep the curved mirror M1 fixed and rotate an intracavity plane mirror M2 at 400 Hz. Because of reflection by mirror M2, the effective rotation rate of M1 is now 800 Hz [13]. As the radius of curvature of the curved mirror M1 is 10 m, the linear sweep speed is $\sim$50 km s^{-1}. The laser mode in the optical cavity is centred on the optic axis and the time taken for this mode to cross the 5 cm diameter mirror is $\sim$1 μs. When the optic axis is along the centre of both the mirrors, the diffraction loss of the multimode beam is the minimum. When the optic axis just enters the edge of the mirrors, or just leaves the mirror edges, the diffraction loss is maximum. The diffraction loss depends on the diameter of the multimode Gaussian laser beam and the extent of Gaussian beam distribution intercepted by the mirrors. This interception factor is known as the cumulative probability function of a standard Gaussian distribution and is available in the form of a table [14]. This table helps in evaluating the varying diffraction losses as the laser beam traverses across the mirrors. The 16 μm laser develops collinearly with the 9.5 μm beam. The 16 μm cavity consists of mirrors M1, M2 and the grating G. During Q-switching the varying diffraction loss due to the movement of the beam along the curved mirror M1 is also applicable to the 16 μm laser beam. However, if the grating is wide, diffraction loss on the grating can be neglected.

4. Method of calculation

The steps leading to the generation of tunable 16 μm radiation from excited CO_2 molecules are as follows:

(1) Excitation of helium-rich gas mixture $CO_2 : N_2 : He::1 : 1 : 40$ in electrical discharge.
(2) Generating Q-switched 9.5 μm pulse through 00^01 to 02^00 transition.
(3) Population inversion between 02^00 and 01^10 levels.
(4) Generation of 16 μm pulse.

The steps listed above first require execution of Boltzmann module for $CO_2 : N_2 : He:: 1 : 1 : 40$ gas mixture which generates data file for ionization rates, attachment rates and drift velocity as a function of E/N. These data are used in Discharge module for solving the rate equations describing current and voltage variations in the discharge. Once current and voltage variations in the discharge are known, the electron number density as a function of time can be evaluated. The electron number density along with excitation rates for CO_2 and N_2 evaluated from Boltzmann module are used in excitation module to calculate the number density of the excited CO_2 molecules at various levels as a function of time. In the last step, Q-switch module is executed to generate circulating intracavity intensity

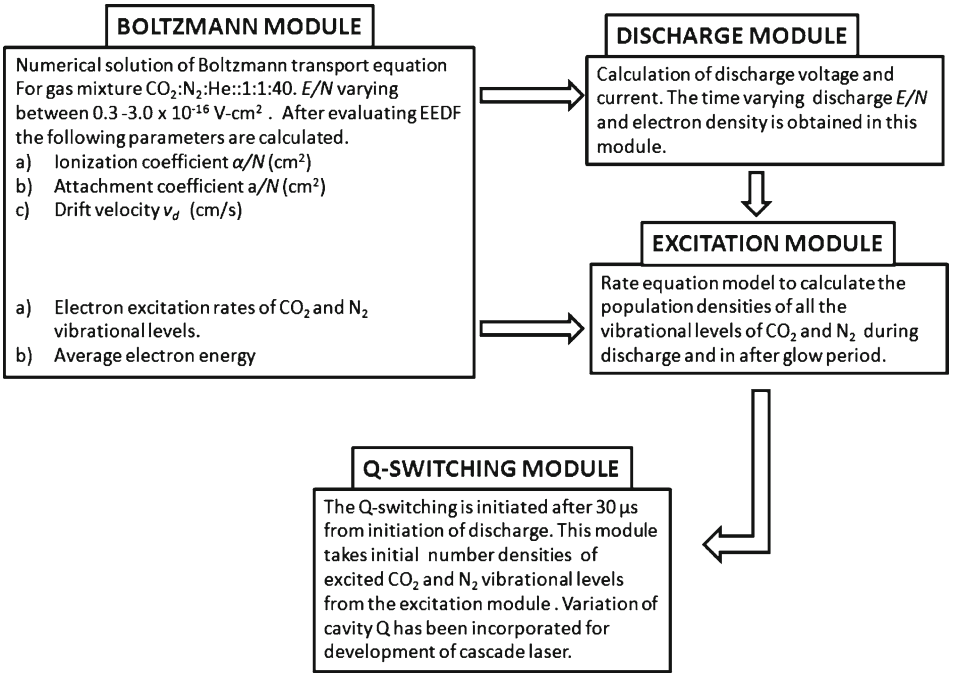

Figure 2. Simulation flow chart for calculating energy and power from cascade laser.

due to Q-switching of 9.5 μm radiation resulting in population inversion between 02^00 and 01^10 levels at low temperatures of active medium. This results in cascade emission of 16 μm radiation. These steps are indicated in the form of simulation flow chart in figure 2. We now explain each module in more detail.

4.1 *Boltzmann module*

In a gas discharge, the electrons are accelerated in the applied electric field and they undergo various elastic and inelastic collisions in the discharge plasma. Depending on the gas mixture and the value of the applied field, the electrons attain a distribution in the energy space, called the electron energy distribution function (EEDF). The Boltzmann module solves [15] the Boltzmann transport equation to predict EEDF for the gas mixture $CO_2 : N_2 : He::1 : 1 : 40$. The rates for various processes which depend on electron kinetics can be determined, if the cross-section of the process and its variation with the energy of the electron are known. Apart from the momentum transfer cross-sections, a total of 34 inelastic collisions with CO_2, N_2 and He gaseous species were used to calculate the EEDF. The EEDF calculated by Boltzmann module was used to calculate α, a and v_d as a function of E/N where E is the electric field between electrodes and N is the neutral particle number density. These data are required by the 'discharge module'. Figure 3 presents variation of α and a as a function of E/N and figure 4 presents the variation of v_d with E/N. The variation of average electron energy ε with E/N is presented in figure 5. The electron impact excitation rates for various levels of CO_2, N_2 and He are also functions of E/N and are governed by EEDF. These rates are available in literature for the conventional CO_2 laser–gas mixtures [16,17] but not for the He-rich mixture used by us. These rates are calculated by the Boltzmann module for the He-rich gas mixture used here.

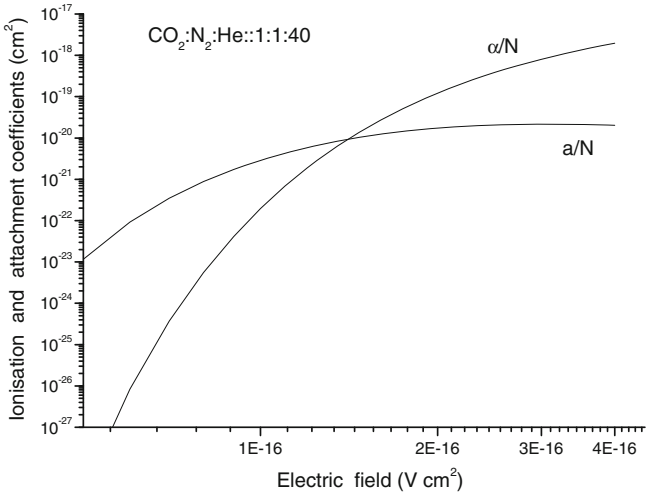

Figure 3. Variation of ionization coefficient (α) and attachment coefficient (a) with E/N.

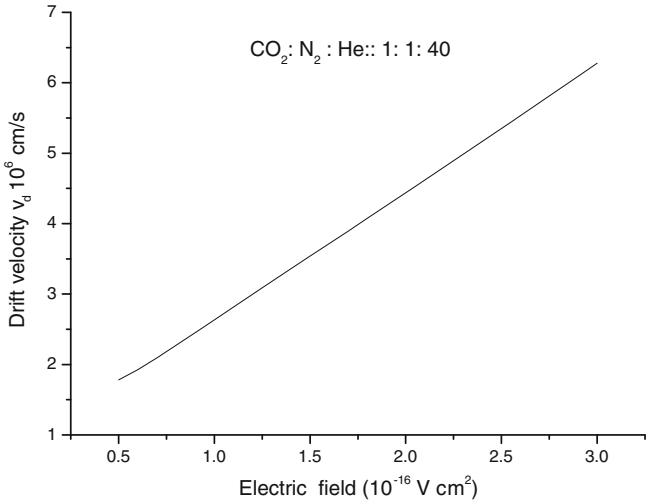

Figure 4. Variation of drift velocity (v_d) with E/N.

4.2 *Discharge module*

In an electron beam-initiated discharge, the initial electrons to start the discharge is provided by an external e-beam. The primary electrons of the beam produce secondary electrons by gas ionization, and provide a source of electrons. These background electrons start the discharge and the discharge once initiated is able to sustain itself even in the

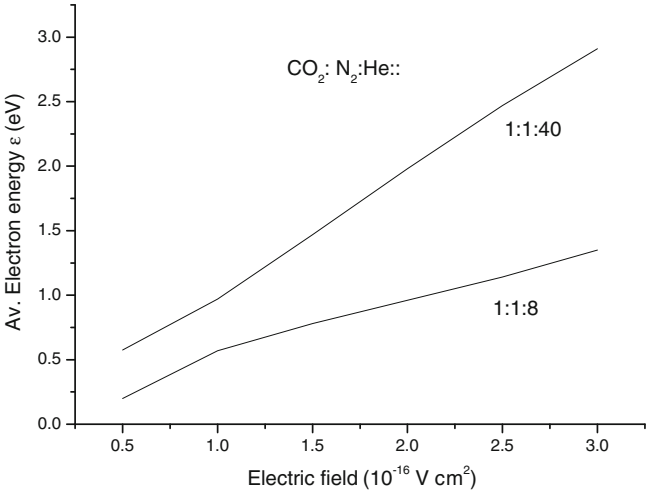

Figure 5. Variation of average electron energy (ε) with E/N for gas mixtures $CO_2 : N_2 : He::1 : 1 : 8$ and $CO_2 : N_2 : He::1 : 1 : 40$.

absence of the e-beam. The rate of change of electron density n_e (cm^{-3}) in the discharge is described by eq. (1).

$$\frac{dn_e}{dt} = S_0 + n_e v_d (\alpha - a) - \gamma n_e^2. \quad (1)$$

Here S_0 is the source term given by [18]

$$S_0 = \frac{j\rho S/\rho}{e_w},$$

where j is the e-beam current density which is equal to 330 mA/cm^2. (s/ρ) is the stopping power of the e-beam by the gas which contains mostly He and it is equal to 3 MeV cm^2/g. Using ρ (density of gas mixture $= 0.022 \times 10^{-3}$ g cm^{-3}) and e_w (ionization potential of CO_2 and N_2 = 32 eV), the value of S_0 is calculated to be 0.46×10^{19} cm^{-3}. In eq. (1), v_d is the drift velocity (cm s^{-1}), α is the ionization coefficient (cm^{-1}), a is the attachment coefficient (cm^{-1}) and γ is the recombination coefficient (cm^3 s^{-1}). As there is no analytical solution of eq. (1), it is solved numerically with the help of Runge–Kutta routine.

The model developed by us to simulate the discharge considers the discharge as a LCR circuit with the discharge plasma as a nonlinear resistance. The change in electron density with time in the discharge is given by eq. (1). The input circuit parameters to the program such as capacitor value, capacitor charging voltage and loop inductance are respectively taken as 0.7 μF, 6 kV and 1 μH. The Boltzman program provides the values of v_d, α and a as a function of E/N. For recombination coefficient we use a value of 10^{-7} cm^3 s^{-1} [18] which is independent of E/N. The discharge cross-sectional area for calculations has been taken as 250 cm^2. The calculations are carried out with time step of 1 ns. At each time step, the field across the discharge is increased from zero in steps of 0.25 V (cm.atm)$^{-1}$ and the electron density and the discharge current are calculated. This operation is continued until the Kirchoff's voltage and current laws in the circuit loop are satisfied. For the next time step, the voltage across the capacitor is adjusted to account for the charge drained from the capacitor in the previous time interval. The calculations are repeated with the updated values of capacitor voltage, electron density and current as the initial values for the next step. Figure 6 depicts the calculated discharge voltage and discharge electron density as a function of time.

4.3 *Excitation module*

This module calculates the population densities in all the vibration levels of CO_2 and N_2, during the discharge and in the afterglow period. The model is an improvisation of the earlier model by Chatterjee and Nath [10]. Figure 7 presents the energy level diagram and indicates the processes which affect the level populations. The rate of change of population densities in the vibration levels can be written as

$$\frac{dn_1}{dt} = (a_1 n_{10} - a_1' n_1) + k(n_{11} n_{10} - n_1 n_{12}) - k_{13} n_1 \quad (2)$$

$$\frac{dn_2}{dt} = (a_2 n_{10} - a_2' n_2) + k_2' (n_2 - n_5) - k_2'' (n_2 - n_4) \quad (3)$$

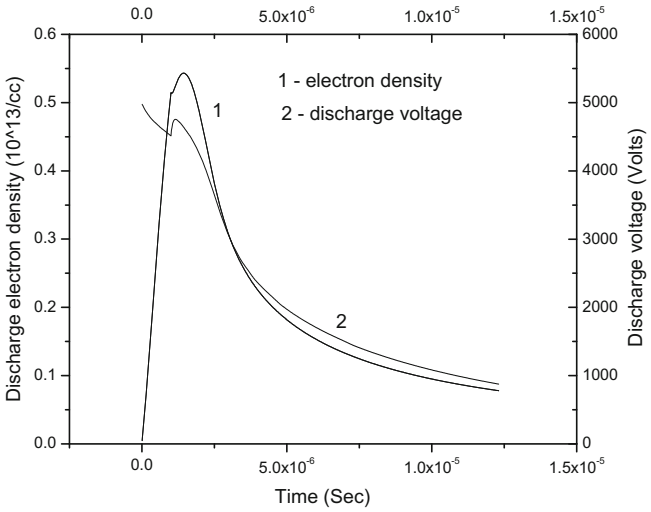

Figure 6. Variation of discharge voltage and electron density in the discharge with time.

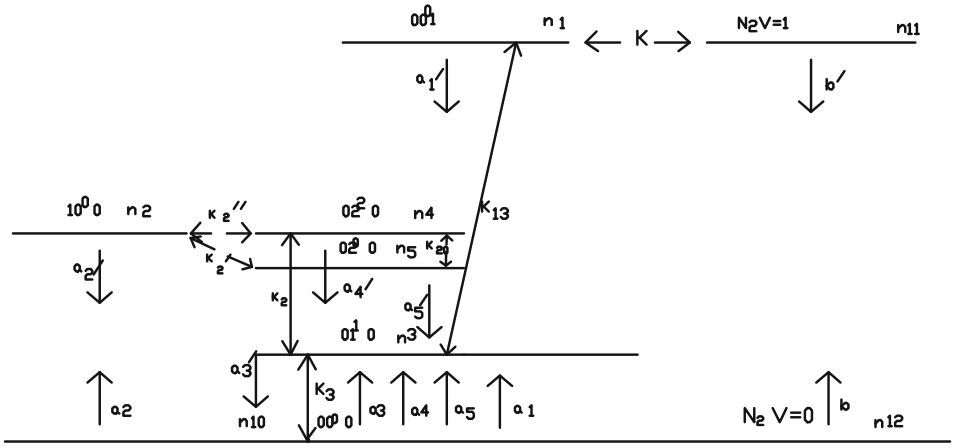

Figure 7. Energy level diagram of CO_2 laser.

$$\frac{dn_3}{dt} = (a_3 n_{10} - a_3' n_3) + k_2\left(n_4 - \frac{n_3^2}{2n_{10}}\right) + k_{13} n_1 - k_3 (n_3 - n_{30}) \quad (4)$$

$$\frac{dn_4}{dt} = (a_4 n_{10} - a_4' n_4) + k_2'' (n_2 - n_4) - k_{20} (n_4 - n_5) - k_2\left(n_4 - \frac{n_3^2}{2n_{10}}\right) \quad (5)$$

$$\frac{dn_5}{dt} = (a_5 n_{10} - a_5' n_5) + k_2' (n_2 - n_5) + k_{20} (n_4 - n_5) \quad (6)$$

$$\frac{dn_{11}}{dt} = (b n_{12} - b' n_{11}) - k (n_{11} n_{10} - n_1 n_{12}) \quad (7)$$

Various symbols used in eqs (2)–(7) are listed in table 1.

Table 1. Various symbols used in eqs (2)–(7).

n_1	Number density of (00^01) level of CO_2, $x = 1$	
n_2	Number density of (10^00) level of CO_2, $x = 2$	
n_3	Number density of (01^10) level of CO_2, $x = 3$	
n_{30}	Thermal population of (01^10) level of CO_2 at 200 K	1.06×10^{15} cm^{-3}
n_4	Number density of (02^20) level of CO_2, $x = 4$	
n_5	Number density of (02^20) level of CO_2, $x = 5$	
n_{10}	Number density of (00^00) level of CO_2, $x = 10$	
n_{11}	Number density of $v = 1$ level of N_2, $x = 11$	
n_{12}	Number density of $v = 0$ level of N_2, $x = 12$	
N_C	Total CO_2 density in the mixture $= n_{10} + n_1 + n_2 + n_5 + 2(n_3 + n_4)$	Constraint used in equation
N_N	Total N_2 density in the mixture $= n_{11} + n_{12}$	Constraint used in equation
n_e	Electron number density	
X_1	Electron excitation rate for (00^01) level of CO_2	Calculated by Boltzmann module
X_2	Electron excitation rate for (10^00) level of CO_2	Calculated by Boltzmann module
X_3	Electron excitation rate for (01^10) level of CO_2	Calculated by Boltzmann module
X_4	Electron excitation rate for (02^20) level of CO_2	Calculated by Boltzmann module
X_5	Electron excitation rate for (02^00) level of CO_2	Calculated by Boltzmann module
X_0	Electron excitation rate for $(v = 1)$ level of N_2	Calculated by Boltzmann module
ε	Average electron energy	Calculated by Boltzmann module
a_x	$n_e X_x$ (s^{-1}) Excitation rate for 'x' level of CO_2 (x = 1–5)	
a'_x	$a_x \exp(\varepsilon_x/\varepsilon)$, De-excitation rate of level 'x' of CO_2	
b	$n_e X_0$ Excitation rate for $v = 1$ level of N_2	
b'	$b \exp(\varepsilon_0/\varepsilon)$, De-excitation rate of $v = 1$ level of N_2	
ε_0	0.29 eV, energy of N_2 vibration level ($v = 1$)	
ε_1	0.29 eV, energy of CO_2 vibration level (00^01)	
ε_2	0.17 eV, energy of CO_2 vibration level (10^00)	
ε_3	0.08 eV, energy of CO_2 vibration level (01^10)	
ε_4	0.16 eV, energy of CO_2 vibration level (02^20)	
ε_5	0.16 eV, energy of CO_2 vibration level (02^00)	
k	Rate of resonance transfer of energy from CO_2 to N_2 at 200 K [19]	6.6×10^{-13} cm^3 part^{-1} s^{-1}
k_3	Relaxation rate for the level (01^10) of CO_2 at 200 K [19]	CO_2: 155 s^{-1} Torr^{-1} N_2: 31 s^{-1} Torr^{-1} He: 3510 s^{-1} Torr^{-1}
k_{13}	Relaxation rate between (00^01) and (01^10) of CO_2 at 200 K [19]	CO_2: 322 s^{-1} Torr^{-1} N_2: 97 s^{-1} Torr^{-1} He: 75 s^{-1} Torr^{-1}
k_2	Relaxation rate between (02^20) and (01^10) of CO_2	4.8×10^5 s^{-1} Torr^{-1} [19]
k_{20}	Relaxation rate between (02^20) and (02^00) of CO_2	4.0×10^5 s^{-1} Torr^{-1} [20]
k''_2	Relaxation rate between (02^20) and (10^00) of CO_2	6.0×10^5 s^{-1} Torr^{-1} [20]
k'_2	Relaxation rate between (02^00) and (10^00) of CO_2	10^6 s^{-1} Torr^{-1} [20]

These equations (eqs (2)–(7)) are solved by Runge–Kutta routine. The calculation is carried out with time step of 1 ns. After the afterglow period, the calculated value of the population density of (00^01) is 0.16×10^{17} cm^{-3}. Thus ∼14% of CO_2 molecules are excited to (00^01) level. The population densities of (02^00) and (01^10) levels are 0.16×10^{14} cm^{-3} and 0.15×10^{16} cm^{-3} respectively. The effective stimulated emission cross-section [21] for the 9.5 μm line is 1.134×10^{-18} cm^2. The effective stimulated emission cross-section $\sigma_{\text{eff}} = P_J \sigma_{ul}$, where P_J is the rotational partition function of the gain medium and its value at 200 K is 0.091 and σ_{ul} is the stimulated emission cross-section at the line centre and its value is 1.246×10^{-17} cm^2. Thus the calculated small signal coefficient which is the product of population inversion between (00^01) and (02^00) levels and effective stimulation cross-section is 1.5% cm^{-1}.

4.4 *Q-Switch module*

The excitation module provides the population densities of all the vibration levels of CO_2 and N_2 at the end of the afterglow period. These are the initial population densities for all the levels to be used in the Q-switch module. The 9.5 μm and the 16 μm transitions are from individual rotational lines. Let us take the specific case of $R(11)$ 16 μm line. In this case the 9.5 μm transition is between $J = 13$ rotation line of (00^01) vibration level and $J = 14$ rotation line of (02^00) vibration level. The 16 μm transition is between $J = 12$ rotation line of (02^00) vibration level and $J = 11$ rotation line of (01^10) vibration level. These transitions are depicted in figure 8.

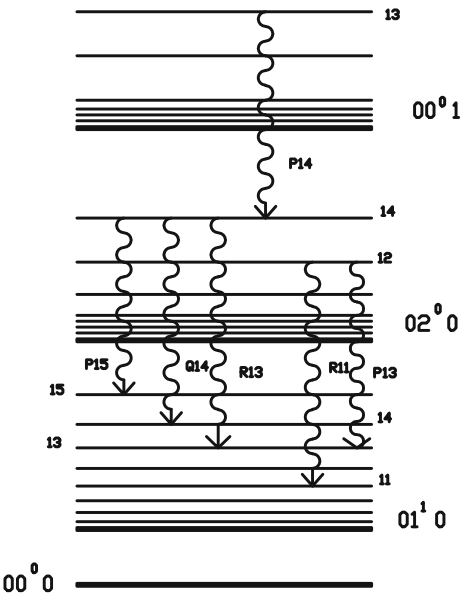

Figure 8. Energy level diagram of CO_2 laser, showing rotational levels and cascade laser transitions.

The population density of the Jth rotation level in kth vibration level is given by

$$n_{Jk} = P_J n_k,$$

where P_J is the rotational partition function $= 0.0028\,(J+1)\exp(-0.0028 \times J(J+1))$.

The new sets of rate equations for evaluating Q-switched radiation in the cavity are as follows:

$$\frac{\mathrm{d}n_1}{\mathrm{d}t} = k(n_{11}n_{10} - n_1 n_{12}) - k_{13}n_1 - S_1 q_1\,(n_{13} - n_{14}) \tag{8}$$

$$\frac{\mathrm{d}n_2}{\mathrm{d}t} = k_2'\,(n_2 - n_5) - k_2''\,(n_2 - n_4) \tag{9}$$

$$\frac{\mathrm{d}n_3}{\mathrm{d}t} = k_2\left(n_4 - \frac{n_3^2}{2n_{10}}\right) + k_{13}n_1 - k_3\,(n_3 - n_{30}) + S_2 q_2\,(n_{15} - n_{16}) \tag{10}$$

$$\frac{\mathrm{d}n_4}{\mathrm{d}t} = k_2''\,(n_2 - n_4) - k_{20}\,(n_4 - n_5) - k_2\left(n_4 - \frac{n_3^2}{2n_{10}}\right) \tag{11}$$

$$\begin{aligned}\frac{\mathrm{d}n_5}{\mathrm{d}t} = {} & k_2'\,(n_2 - n_5) + k_{20}\,(n_4 - n_5) \\ & + S_1 q_1\,(n_{13} - n_{14}) - S_2 q_2\,(n_{15} - n_{16})\end{aligned} \tag{12}$$

$$\frac{\mathrm{d}n_{11}}{\mathrm{d}t} = k\,(n_{11}n_{10} - n_1 n_{12}) \tag{13}$$

$$\frac{\mathrm{d}n_{13}}{\mathrm{d}t} = -S_1 q_1\,(n_{13} - n_{14}) + \left(\frac{(P_J n_1 - n_{13})}{\tau_r}\right), \quad \text{for } J = 13 \tag{14}$$

$$\frac{\mathrm{d}n_{14}}{\mathrm{d}t} = S_1 q_1\,(n_{13} - n_{14}) + \left(\frac{(P_J n_5 - n_{14})}{\tau_r}\right), \quad \text{for } J = 14 \tag{15}$$

$$\frac{\mathrm{d}n_{15}}{\mathrm{d}t} = -S_2 q_2\,(n_{15} - n_{16}) + \left(\frac{(P_J n_5 - n_{15})}{\tau_r}\right), \quad \text{for } J = 12 \tag{16}$$

$$\frac{\mathrm{d}n_{16}}{\mathrm{d}t} = S_2 q_2\,(n_{15} - n_{16}) + \left(\frac{(P_J n_3 - n_{16})}{\tau_r}\right), \quad \text{for } J = 11 \tag{17}$$

Various symbols used in eqs (8)–(17) are listed in table 2.

Stimulated emission rate for the specific transition is $S_j = (cl\sigma_{ulj}/L)$, where c is the velocity of light, l is the length of the discharge (150 cm) and L is the length of the optical cavity (500 cm) and $\sigma_{ulj} = (\lambda_j^2 A_j/4\pi^2\Delta\nu)$, where λ_j is the laser wavelength, $A_j = 0.34\ \mathrm{s}^{-1}$ for 9.5 μm radiation and $0.48\ \mathrm{s}^{-1}$ for 16 μm radiation [22]. The pressure broadened linewidth $\Delta\nu$ can be calculated to be 629 MHz with the data provided by Manes and Seguin [23]. The second term in the RHS of the last four equations (eqs (14)–(17)) represents population change due to rotational relaxation.

Table 2. Various symbols used in eqs (8)–(17).

n_{13}	Number density of rotation level $J = 13$ in (00^01)	
n_{14}	Number density of rotation level $J = 14$ in (02^00)	
n_{15}	Number density of rotation level $J = 12$ in (02^00)	
n_{16}	Number density of rotation level $J = 11$ in (01^10)	
n_{13i}	Starting value of population density of level ($J = 13$) of 00^01	$2P_{13}n_{1i}$*
n_{14i}	Starting value of population density of level ($J = 14$) of 02^00	$2P_{14}\,n_{5i}$
n_{15i}	Starting value of population density of level ($J = 12$) of 02^00	$2P_{12}\,n_{5i}$
n_{16i}	Starting value of population density of level ($J = 11$) of 01^10	$P_{11}\,n_{3i}$
S_1	Stimulation emission rate for 9.5 μm radiation	$S_1 = \frac{c\,l\,\sigma_{ul1}}{L}$
S_2	Stimulation emission rate for 16 μm radiation	$S_2 = \frac{c\,l\,\sigma_{ul2}}{L}$
q_1	Photon density of 9.5 μm radiation	
q_2	Photon density of 16 μm radiation	
τ_r	Rotational relaxation rate	

*The subscript i denotes values of population densities of levels.

The rate equations describing the build-up of photon densities in the cavity are [21]:

$$\frac{dq_1}{dt} = S_1 q_1 (n_{13} - n_{14}) - W_1 q_1 + D_1 n_{13}, \tag{18}$$

$$\frac{dq_2}{dt} = S_1 q_2 (n_{15} - n_{16}) - W_2 q_2 + D_2 n_{15}, \tag{19}$$

where W_1 is the reciprocal of cavity decay time for 9.5 μm laser and is given by

$$W_1 = \frac{c}{2l}\left(T_{\text{loss}} - \ln(R_1 R_2 P R_1 P R_2)\right). \tag{20}$$

Here $T_{\text{loss}} = 0.1$ which represents the loss in the Brewster windows used in the laser chamber, R_1 is the reflectivity of mirror M1 and is equal to 1.0 whereas R_2 is the reflectivity of the output coupler and its value is 0.98. PR_1 and PR_2 determine the variation of cavity Q (interception factor) with rotation of mirror M2. As explained in Q-switch module, these factors represent the interception of the Gaussian laser beam by the two end mirrors as the laser mode sweeps across these mirrors. The estimated laser mode diameters at curved mirror M1 and plane output coupler OC are respectively 22 and 15.6 mm. The average mode diameter can be calculated to be 18 mm [12]. As the optic axis of the mode enters the edge of mirror M1, the maximum diffraction loss is 50%. When the optic axis of the mode is centred on mirror M1, the diffraction loss is minimum, as the mirror intercepts most of the Gaussian beam with its wings. PR_1 can be calculated with the help of the table of cumulative distribution function of Gaussian beams [14]. The minimum diffraction loss is found to be 2.3%, corresponding to a value of 0.977 for PR_1. We use 1 ns as the time step for our calculations. The calculation starts with the optic axis entering the edge of the mirror. From the sweep speed we know the distance by which the laser mode advances on the mirror and can calculate PR_1 for each time step. Such a table was prepared for PR_1 and subsequently used during the execution of the program. Similarly, PR_2 is the interception factor for the laser mode by the output coupler OC. In this case the

minimum diffraction loss is 0.14%, corresponding to a value of 0.9986 for PR_2. Again PR_2 was calculated for each time step and listed in a table and these values are used in the calculation.

For the 16 μm laser the reciprocal of cavity decay time W_2 is given by

$$W_2 = \frac{c}{2l}\left(T_{\text{loss}} - \ln(R_1 R_3 P R_1)\right). \tag{21}$$

Here R_3 is the effective reflectivity of the grating. Since the output coupling is 10% from a grating with 85% efficiency, $R_3 = 0.9 \times 0.85 = 0.765$. The 16 μm and the 9.5 μm beams are collinear and are of the same size. If one uses a wide grating, the diffraction loss on the grating can be neglected. The factors D_j in eqs (18) and (19) are the spontaneous emission rates given by the expression [21]

$$D_j = \frac{\lambda_j^2}{A_{\text{L}}}\frac{\mathrm{d}v_j}{\Delta\nu}\frac{A_j}{\pi}.$$

Here A_{L} is the cross-sectional area of the laser beam and $\mathrm{d}\nu$ is the inverse radiative lifetime of the lasing transition which is given by $dv_j = W_j/2\pi$. The 12 rate equations given in eqs (8)–(19) were solved by Runge–Kutta routine to calculate the cascade laser photon densities.

5. Results and discussions

The results are presented in table 3. We present three cases. In each one, the stimulating laser operates on 9.6 $P(14)$ line, and the 16 μm lasing has been calculated for the $Q(14)$, $P(13)$ and $R(11)$ lines. Table 3 lists starting and terminating J numbers for the rotational levels of transitions, their wavelengths and wave numbers. The peak power and energy of 16 μm laser and its efficiency are also shown in the same table. In all these cases, total energy dissipated in the discharge is 37.5 J. The efficiency is defined as the ratio of the

Table 3. Energy and power of cascade laser lines.

S.No.	Cascade laser lines	Transition	Wavelength (μm)	Wavenumber (cm^{-1})	Peak power (kW)	Energy (mJ)	Efficiency (%)
1	$P(14)$	$00^0 1J = 13$ $\rightarrow 02^0 0J = 14$	9.498	1052.85	20.7	8.8	
	$Q(14)$	$02^0 0J = 14$ $\rightarrow 01^1 0J = 14$	16.176	618.2	42.9	8.4	0.02
2	$P(14)$	$00^0 1J = 13$ $\rightarrow 02^0 0J = 14$	9.498	1052.85	20.7	8.3	
	$P(13)$	$02^0 0J=12$ $\rightarrow 01^1 0J = 13$	16.446	608.1	29.1	6.5	0.017
3	$P(14)$	$00^0 1J = 13$ $\rightarrow 02^0 0J = 14$	9.498	1052.85	20.7	7.9	
	$R(11)$	$02^0 0J = 12$ $\rightarrow 01^1 0J = 11$	15.935	627.6	24.7	5.2	0.014

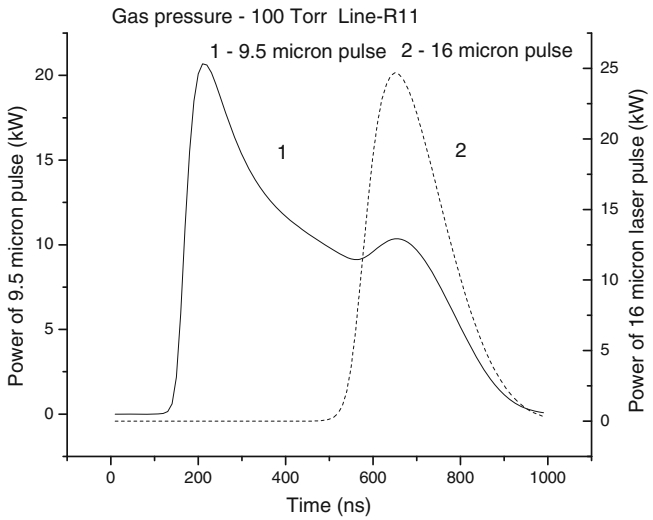

Figure 9. The calculated pulse shapes and amplitudes of the cascade laser.

16 μm laser energy and the discharge energy. The Q line is the strongest and P lines are stronger than the R lines. It may be pointed out that we are considering such P and R lines, where the 9.6 μm line and the 16 μm lines are not connected. Lines are connected when the terminating J number of the 9.6 μm radiation is the same as the originating J number of the 16 μm radiation, as in the case of the $Q(14)$ line. For weak P and R lines, it may be beneficial to tune the stimulating 9.6 μm line and connect it with the desired P or R line. Experimentally also it is easy to implement this by replacing the output coupler OC by a grating. The calculated cascade laser pulse shapes are shown in figure 9.

Table 4. Comparison of operating parameters of our scheme with those of Sakai and Hamada [11].

Parameters	Our system	Sakai and Hamada
Type	E-beam initiated pulsed laser	RF excited pulsed laser
Gas mixture, CO_2:N_2:He	1 : 1 : 40	1 : 1.4 : 7.6
Gas pressure (Torr)	100	100
Gas temperature (K)	200	350
Discharge length (m)	1.5	2.24
Cavity length (m)	5	6
Small signal gain coeff. (cm^{-1})	1.5%	1%
Beam diameter (mm)	18	18
Output power (kW)	20	500
Output coupling	2%	50%
Wavelength (μm)	9.5	10.6
Intracavity peak power (kW)	1000	1000

Sakai and Hamada [11] have carried out Q-switching in a RF excited fast longitudinal flow pulsed CO_2 laser. Table 4 lists a comparison of the operating parameters of their laser with those of our proposed scheme. Though the laser systems are different, there are several similarities of operating parameters in the two systems. The intracavity power of the Q-switched pulse generated in the two systems is the same. If we increase our discharge length to 2.24 m and cavity length to 6 m, to mimic the experimental conditions of Sakai and Hamada, the internal power of the 9.5 μm radiation increases to 1.3 MW. Sakai and Hamada have developed an analytical model. This model predicts the power of the laser as a function of small signal gain. Our calculated intracavity power of the 9.5 μm radiation matches well with the analytical prediction of Sakai and Hamada. Hence we conclude that the theoretical predictions of our program are realistic and practically realizable.

The advantage of our scheme is its scalability and ability to generate high power and energy at 16 μm. Kasner *et al* [7] reported 16 μm energies of 15–20 μJ. In its present configuration, our scheme is capable of generating 16 μm output energies greater than 5 mJ. Such a laser can find application in laser isotope separation. For selective vibrational excitation (in the $\nu 3$ band) of $^{235}UF_6$ by 'Q-slope approach' [3] and its scavenging by a suitable chemical reagent [4], laser operating between 627 and 628 cm^{-1} is required. The $R(11)$ line operating on 627.6 cm^{-1} is an appropriate candidate. The laser head requires cryogenic cooling. This can be achieved by closed loop gas circulation schemes normally used for CO lasers [24]. The laser also requires repetitive rate operation. For the electron beam-controlled discharge module, the repetition rate is dictated by foil heating. For the parameters presented in this paper the discharge module can be easily operated at 100 Hz [18].

6. Conclusion

We have presented a scheme for a cascade lasing system utilizing rotating mirror Q-switching. The optical arrangement allows independent tuning of the two cascade laser beams. The energy and power for the three 16 μm lines $Q14$, $P13$ and $R11$, were calculated by a theoretical model developed by us. We have compared our theoretical prediction regarding the generation of the Q-switched 9.5 μm pulse with experimental results of a high-power Q-switched CO_2 laser. The 16 μm laser lines generated by our scheme have sufficient energy, power and repetition rate to find application in laser isotope separation experiments.

References

[1] R M Osgood, *Appl. Phys. Lett.* **32(9)**, 564 (1978)
[2] V S Letokhov and C B Moore, *Sov. J. Quantum Electron.* **6**, 129 (1976)
[3] J A Eerkens, *Appl. Phys.* **10**, 15 (1976)
[4] J A Horsely, P Rabinowitz, A Stein, D M Cox, R O Brickman and A Kaldor, *IEEE J. Quantum Electron.* **QE-16(11)**, 412 (1980)
[5] R L Wexler, T J Mannucia and R W Wayant, *Appl. Phys. Lett.* **31**, 730 (1977)
[6] W F Krupke, US Patent No. 4,053,851 (1977)

[7] W H Kasner, L D Pleasance and L H Taylor, *IEEE/OSA Conference on Laser Engineering and Applications* (Washington, DC, 1977)
[8] W H Kasner, US Patent No. 4,238,741 (1980)
[9] U Nundy, *Pramana – J. Phys.* **75(5)**, 895 (2010)
[10] U K Chatterjee and A K Nath, *J. Appl. Phys.* **53**, 4610 (1982)
[11] T Sakai and N Hamada, *Jpn. J. Appl. Phys.* **35**, 3428 (1996)
[12] U Nundy and U K Chatterjee, *J. Appl. Phys.* **53(12)**, 8501 (1982)
[13] Y-C Qu, X-Y Hu, F-M Liu, D-M Ren and J-S Zhao, *Infrared Physics & Technology* **41**, 139 (2000)
[14] K F Riley, M P Hobson and S J Bence, *Mathematical methods for physics and engineering, table of cumulative probability function for standard Gaussian distribution* (Cambridge University Press, 1998) p. 901
[15] M Kumar, J Khare and A K Nath, *Opt. Laser Technol.* **39**, 86 (2007)
[16] O P Judd, *J. Appl. Phys.* **45(10)**, 4572 (1974)
[17] J J Lowke, A V Phelps and B W Irwin, *J. Appl. Phys.* **44(10)**, 4664 (1973)
[18] J D Daughtery, in: *Principles of laser plasma* edited by G Bekefi (Wiley, New York, 1976) p. 370
[19] R Taylor and S Bitterman, *Rev. Mod. Phys.* **41(1)**, 26 (1969)
[20] D C Tyte, *Advances in quantum electronics* edited by D W Goodwin (Academic Press, London, 1970) Vol. 1, p. 129
[21] J Gilbert, J L Lachambre, F Rheault and R Fortin, *Can. J. Phys*. **50**, 2523 (1972)
[22] H Statz, C L Tang and G F Koster, *J. Appl. Phys.* **37(10)**, 4278 (1966)
[23] K R Manes and H J Seguin, *J. Appl. Phys.* **43(12)**, 5073 (1972)
[24] A A Ionin, *Quantum Electron* **23(2)**, 9 (1993)